

The following resources related to this article are available online at www.sciencemag.org (this information is current as of December 3, 2009):

Updated information and services, including high-resolution figures, can be found in the online version of this article at:

<http://www.sciencemag.org/cgi/content/full/310/5756/1966>

Supporting Online Material can be found at:

<http://www.sciencemag.org/cgi/content/full/310/5756/1966/DC1>

A list of selected additional articles on the Science Web sites **related to this article** can be found at:

<http://www.sciencemag.org/cgi/content/full/310/5756/1966#related-content>

This article **cites 23 articles**, 9 of which can be accessed for free:

<http://www.sciencemag.org/cgi/content/full/310/5756/1966#otherarticles>

This article has been **cited by** 106 article(s) on the ISI Web of Science.

This article has been **cited by** 39 articles hosted by HighWire Press; see:

<http://www.sciencemag.org/cgi/content/full/310/5756/1966#otherarticles>

This article appears in the following **subject collections**:

Medicine, Diseases

<http://www.sciencemag.org/cgi/collection/medicine>

Information about obtaining **reprints** of this article or about obtaining **permission to reproduce this article** in whole or in part can be found at:

<http://www.sciencemag.org/about/permissions.dtl>

the anticipatory rise in category-selective activity shown in Fig. 2 (figs. S10 and S11). Taken together, these results suggest that including voxels outside of the peak category-selective ROIs improves our ability to detect subtle changes in the reinstatement of category-related activity.

The work described here is one of a growing number of fMRI studies illustrating the benefits of multivoxel pattern-classification techniques (17–20, 25, 26). These studies have demonstrated that, by efficiently extracting the information present in multivoxel patterns of brain activity, it is possible to detect subtle distinctions between cognitive states using relatively thin time slices of brain data (on the order of seconds). Whereas previous applications of classification techniques have focused on brain activity elicited by specific perceptual cues, our study shows that classification algorithms can be used to extract a time-varying trace of the subjects' cognitive state as they search through memory in the absence of specific cues. Our results ground Tulving's speculations about mental time travel in neural fact. As subjects search for memories from a particular event, their brain state progressively comes to resemble their brain state during the sought-after event, and the degree of match predicts what kinds of information the subjects will retrieve. By providing a direct view of how subjects are cueing memory, the methods presented here constitute a powerful new tool that researchers can use to test and refine theories of how people mine the recesses of the past.

References and Notes

1. J. L. McClelland, D. E. Rumelhart, in *Parallel Distributed Processing: Explorations in the Microstructure of Cognition*, J. L. McClelland, D. E. Rumelhart, PDP Research Group, Eds. (Massachusetts Institute of Technology Press, Cambridge, MA, 1986), vol. 2, chap. 17, p. 170.
2. J. L. McClelland, in *Memory Distortion: How Minds, Brains, and Societies Reconstruct the Past*, D. L. Schacter, Ed. (Harvard Univ. Press, Cambridge, MA, 1995), chap. 2, p. 69.
3. E. Tulving, *Curr. Dir. Psychol. Sci.* **2**, 67 (1993).
4. K. A. Norman, D. L. Schacter, *Implicit Memory and Metacognition*, L. M. Reder, Ed. (Erlbaum, Hillsdale, NJ, 1996).
5. M. W. Howard, M. J. Kahana, *J. Math. Psychol.* **46**, 269 (2002).
6. E. Tulving, D. Thompson, *Psychol. Rev.* **80**, 352 (1973).
7. F. C. Bartlett, *Remembering: A Study in Experimental and Social Psychology* (Cambridge Univ. Press, Cambridge, 1932).
8. L. Sahakyan, C. M. Kelley, *J. Exp. Psychol. Learn. Mem. Cogn.* **28**, 1064 (2002).
9. S. M. Smith, in *Memory in Context: Context in Memory*, G. M. Davies, D. M. Thomson, Eds. (Wiley, Oxford, UK, 1988), pp. 13–34.
10. M. W. Howard, M. J. Kahana, *J. Exp. Psychol. Learn. Mem. Cogn.* **25**, 923 (1999).
11. M. E. Wheeler, S. E. Petersen, R. L. Buckner, *Proc. Natl. Acad. Sci. U.S.A.* **97**, 11125 (2000).
12. L. Nyberg, R. Habib, E. Tulving, *Proc. Natl. Acad. Sci. U.S.A.* **97**, 11120 (2000).
13. M. E. Wheeler, R. L. Buckner, *J. Neurosci.* **23**, 3869 (2003).
14. I. Kahn, L. Davachi, A. D. Wagner, *J. Neurosci.* **24**, 4172 (2004).

15. A. P. R. Smith, R. N. A. Henson, R. J. Dolan, M. D. Rugg, *Neuroimage* **22**, 868 (2004).
16. R. Shiffrin, R. Ratcliff, S. Clark, *J. Exp. Psychol. Learn. Mem. Cogn.* **16**, 179 (1990).
17. J. V. Haxby et al., *Science* **293**, 2425 (2001).
18. T. M. Mitchell et al., *Mach. Learn.* **5**, 145 (2004).
19. S. J. Hanson, T. Matsuka, J. V. Haxby, *Neuroimage* **23**, 156 (2004).
20. D. D. Cox, R. L. Savoy, *Neuroimage* **19**, 261 (2003).
21. Materials and methods—including behavioral paradigm, scanning parameters, classifier methods, data preprocessing details, details regarding nonparametric statistics, and details of map creation—are available as supporting material on Science Online.
22. N. Kanwisher, J. McDermott, M. M. Chun, *J. Neurosci.* **17**, 4302 (1997).
23. R. Epstein, N. Kanwisher, *Nature* **392**, 598 (1998).
24. A listing of the brain regions that were most reliably activated by each study context across subjects (as identified by a group general linear model analysis) is available (21).
25. Y. Kamitani, F. Tong, *Nat. Neurosci.* **8**, 679 (2005).
26. J. D. Haynes, G. Rees, *Nat. Neurosci.* **8**, 686 (2005).
27. When computing the correlation between classifier estimates and recall behavior, we adjusted for the hemodynamic response in two ways. In our primary analysis, we shifted the recall record forward by three time points (as in Fig. 1). We also ran a secondary analysis, where we convolved the recall record with a model of the hemodynamic response. The two analyses yielded very similar results (21).
28. The following example details how a set of hypothetical recall events are assigned to the currently recalled, recently recalled, and baseline plots. Assume that a subject recalls nothing for 20 s, then recalls a location ("Taj Mahal"), then recalls a face ("Bruce Lee") 5 s after recalling the location. The location recall ("Taj Mahal") qualifies for inclusion in the

event-related average, because no other locations were recalled in the preceding 14.4 s. For the location recall, the currently recalled category is location, and both the face and object categories are assigned to the baseline plot (because neither faces nor objects were recalled in the 14.4 s preceding the location recall). The face recall ("Bruce Lee") also qualifies for inclusion in the event-related average, because no other faces were recalled in the preceding 14.4 s. With regard to the face recall, the currently recalled category is face; the location category is assigned to the recently recalled plot, because a location item was recalled during the 14.4 s preceding the face recall; and the object category is assigned to the baseline plot, because no items were recalled from that category in the 14.4 s preceding the face recall.

29. This study was supported by grants from the National Institute of Mental Health (NIMH) to K.A.N. (R01MH069456) and to J.D.C. (R01MH052864). S.M.P. was supported by a Ruth L. Kirschstein National Research Service Award predoctoral fellowship from NIMH (MH070177-01). Special thanks to R. Schapiro, J. Haxby, P. Sederberg, and M. Kahana for comments; to C. Buck for assisting with running the subjects; and to S. Takerkart and L. Nyström for assistance with the analysis.

Supporting Online Material

www.sciencemag.org/cgi/content/full/310/5756/1963/DC1
 Materials and Methods
 SOM Text
 Figs. S1 to S11
 Tables S1 to S8
 References

19 July 2005; accepted 11 November 2005
 10.1126/science.1117645

Inducible Nitric Oxide Synthase Binds, S-Nitrosylates, and Activates Cyclooxygenase-2

Sangwon F. Kim,¹ Daniel A. Huri,¹ Solomon H. Snyder^{1,2,3*}

Cyclooxygenase-2 (COX-2) and inducible nitric oxide synthase (iNOS) are two major inflammatory mediators. Here we show that iNOS specifically binds to COX-2 and S-nitrosylates it, enhancing COX-2 catalytic activity. Selectively disrupting iNOS–COX-2 binding prevented NO-mediated activation of COX-2. This synergistic molecular interaction between two inflammatory systems may inform the development of anti-inflammatory drugs.

Inflammatory processes are mediated by multiple molecular mechanisms. Two of the most prominent are the production of nitric oxide (NO) by inducible NO synthase (iNOS) and the formation of prostaglandins by cyclooxygenase-2 (COX-2; prostaglandin H₂ synthase) (1, 2). COX-2 inhibitors have attained widespread use as anti-inflammatory agents, although they elicit potentially adverse side effects (1, 3, 4), whereas iNOS inhibitors are not presently employed therapeutically. Inflammatory stimuli

elicit the synthesis of iNOS and COX-2 proteins with similar time courses, which suggests that the two systems may interact (5, 6). Stimulants of iNOS such as bradykinin (7) and lipopolysaccharide (LPS) plus interferon-γ (IFN-γ), two components of endotoxin, enhance prostaglandin formation (8). NOS inhibitors prevent the formation of prostaglandins (9).

To determine whether iNOS and COX-2 interact, we used a murine macrophage cell line (RAW264.7) in which LPS and IFN-γ massively activate both iNOS and COX-2. iNOS immunoprecipitated with COX-2-specific antibodies from lysates of cells treated with LPS-IFN-γ (Fig. 1A). This was also observed in transfected human embryonic kidney cells (HEK293T) overexpressing both proteins (fig. S1A). The two enzymes also coimmuno-

¹Department of Neuroscience, ²Department of Pharmacology and Molecular Sciences, and ³Department of Psychiatry and Behavioral Sciences, The Johns Hopkins University School of Medicine, 725 North Wolfe Street, Baltimore, MD 21205, USA.

*To whom correspondence should be addressed. E-mail: ssnyder@jhmi.edu

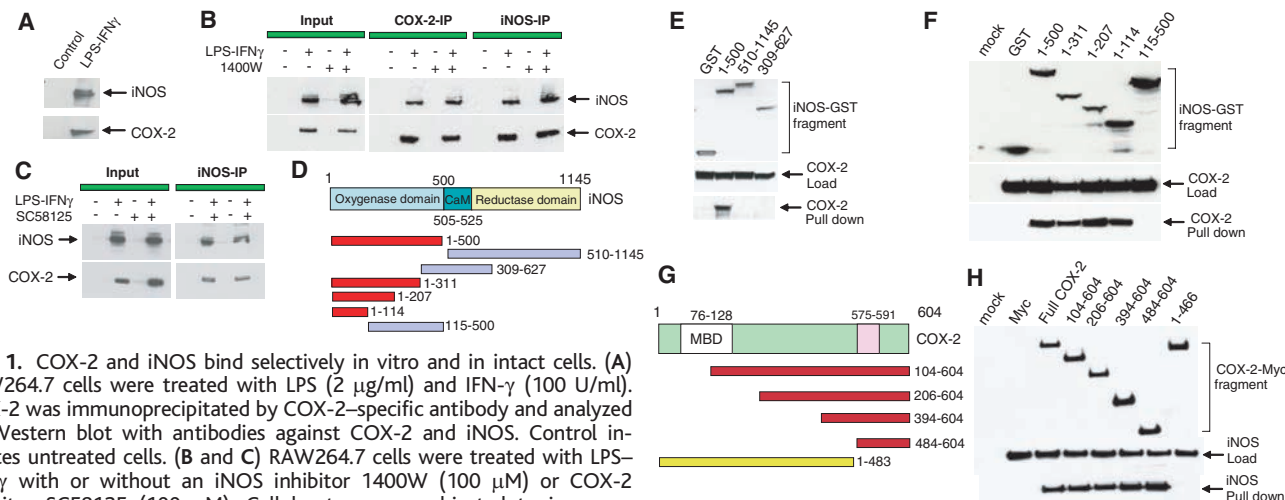


Fig. 1. COX-2 and iNOS bind selectively in vitro and in intact cells. (A) RAW264.7 cells were treated with LPS (2 μg/ml) and IFN-γ (100 U/ml). COX-2 was immunoprecipitated by COX-2-specific antibody and analyzed by Western blot with antibodies against COX-2 and iNOS. Control indicates untreated cells. (B and C) RAW264.7 cells were treated with LPS-IFN-γ with or without an iNOS inhibitor 1400W (100 μM) or COX-2 inhibitor SC58125 (100 μM). Cell lysates were subjected to immunoprecipitation (IP) and Western blot analysis with antibodies against COX-2 and iNOS. (D) The fragments of iNOS denoted in red bind to full-length COX-2, whereas fragments labeled purple do not, as determined by coimmunoprecipitation of full-length COX-2 by iNOS fragment fused to glutathione S-transferase (GST). The numbers represent the number of the amino acid sequence. (E) Transfected HEK293T cells expressing COX-2 and iNOS fragments expressed as fusion proteins with GST were precipitated with glutathione-conjugated beads. Proteins were detected by Western blot with antibodies against GST or COX-2. (F) Transfected HEK293T cells

expressing COX-2 and epitope-tagged (Myc) iNOS fragments were immunoprecipitated with Myc-specific antibody and then analyzed by Western blot. (mock: The cells were treated with transfection reagent without the plasmid.) (G) Generated fragments of COX-2 that bind to full-length iNOS are labeled in red; those that do not bind are labeled in yellow. (MBD, membrane-binding domain). (H) Transfected HEK293T cells expressing iNOS and Myc-tagged COX-2 fragments were immunoprecipitated with Myc-specific antibody and analyzed by Western blot. (mock: The cells were treated with transfection reagent without the plasmid.)

precipitated from peritoneal macrophages obtained from mice injected with thioglycollate, an inflammatory stimulus that induces peritonitis or pleuritis (fig. S1B). To determine whether catalytic activity of the enzymes influences their interactions, cells that were induced by LPS-IFN-γ were also treated with the iNOS-selective inhibitor 1400W (Fig. 1B) or the COX-2-selective inhibitor SC58125 (Fig. 1C). Coimmunoprecipitation of iNOS and COX-2 by antibodies specific to either protein was unaffected by either inhibitor. The binding of iNOS and COX-2 was selective, because COX-1 did not immunoprecipitate with iNOS. To map the binding sites on both proteins, we generated selective deletions of iNOS (Fig. 1, D to F) and COX-2 (Fig. 1, G and H) sequences. The amino acid segment 1 to 144 of iNOS, which is within the oxygenase domain, is required, whereas the C terminus of COX-2 mediates binding and includes amino acids 484 to 604, which do not exist in COX-1.

The two major mechanisms whereby NO influences its intracellular targets are stimulation of guanylyl cyclase by direct binding of NO to iron in heme at the active site of guanylyl cyclase (10) or S-nitrosylation of protein targets on appropriate cysteines (11, 12). Because COX-2 has heme at its active site (13), this would be a potential target. However, NO binding to heme in COX-1 does not alter its activity (14). COX-2 also contains 13 cysteines whose roles are not fully understood (15). To explore the possibility of S-nitrosylation of COX-2 by NO, we examined multiple NO donors including nitroso-S-glutathione (GSNO) (Fig. 2A), sodium nitroprusside (SNP), spermine-NO, and

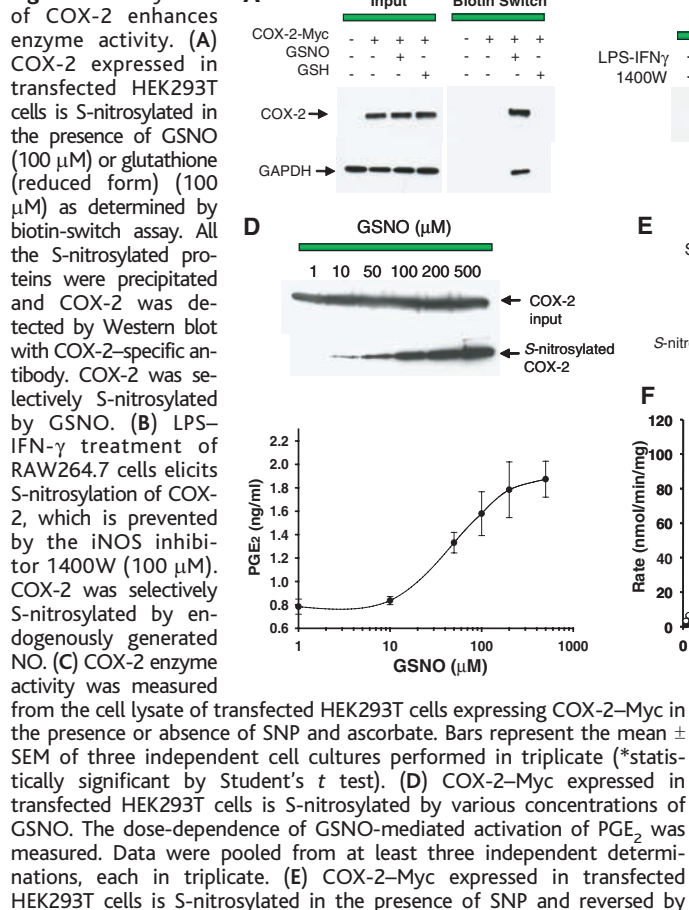
(Z)-1-[N-(2-aminoethyl)-N-(2-ammonioethyl) amino]diazene-1-ium-1,2-diolate (DETA-NONOate) (fig. S3A). Using the biotin switch method in which all the S-nitrosylated cysteines are selectively biotinylated (16), we observed that all four NO donors elicited S-nitrosylation of COX-2 in transfected HEK293T cells expressing COX-2-Myc (Fig. 2A). S-Nitrosylation of COX-2 was also observed in RAW264.7 cells treated with LPS-IFN-γ. This was prevented when cells were treated with iNOS inhibitor 1400W (Fig. 2B and fig. S3B). The biotin switch method was specific, as H₂O₂ did not elicit S-nitrosylation (fig. S4). We also ruled out the possibility that sulfenic acid modification was detected by the biotin switch assay by demonstrating that arsenite, which reverses sulfenic acid modifications but not S-nitrosylation, failed to provide the biotin switch signal afforded by ascorbate using GSNO with purified COX-2 or LPS-IFN-γ treatment of RAW 264.7 cells (fig. S4B). In some instances there may be no need to deliver NO directly to targets, as some actions of NO are prevented by hemoglobin, which sequesters freely diffusible NO (17). We examined the effects of hemoglobin on S-nitrosylation of COX-2 under varying conditions. In transfected HEK293T cells expressing COX-2, hemoglobin prevented the S-nitrosylation elicited by GSNO (fig. S5A), whereas it failed to alter S-nitrosylation of COX-2 in RAW264.7 cells activated by LPS-IFN-γ (fig. S5B). Thus, in the more physiologic macrophage cell line, the S-nitrosylation of COX-2 induced by an inflammatory stimulus does not appear to be elicited by freely diffusible NO.

To determine whether S-nitrosylation of COX-2 alters enzyme activity, we examined transfected HEK293T cells expressing COX-2-Myc. The NO donor SNP, added to cell lysates, elicited a twofold increase in COX-2 activity, reflecting S-nitrosylation. Ascorbic acid reversed S-nitrosylation (16, 18) and prevented the increase (Fig. 2, C and D). The reversal by ascorbate of COX-2 activation by NO donors is not merely a reflection of ascorbate influences on enzyme substrates or intermediate products, as ascorbate failed to affect COX-2 activity in preparations not treated with SNP. Further evidence that S-nitrosylation and COX-2 activation are related is the closely similar concentration-response relation between the effects of the NO donor GSNO on S-nitrosylation and on COX-2 activity (Fig. 2E).

NO activates COX-2 by increasing its apparent V_{max} without changing its K_m (Fig. 2F). The higher concentration of SNP required to activate COX-2 in vitro compared with intact cells accords with earlier studies showing greater potency of NO donors in intact cells (19). To ascertain the kinetic basis for NO activation of COX-2, we conducted enzyme assays with increasing concentrations of sucrose to augment viscosity and slow down enzyme kinetics (Fig. 2G). As expected, with increasing viscosity, the ratio of control enzyme activity to the activity in more viscous solutions increased. This increase was diminished in SNP samples, consistent with SNP's accelerating the release of product from the enzyme.

To determine which of the 13 cysteines of COX-2 are critical for the augmentation of COX-2 activity elicited by S-nitrosylation,

Fig. 2. S-Nitrosylation of COX-2 enhances enzyme activity.



the addition of ASC. All the S-nitrosylated proteins were precipitated, and COX-2 was detected by Western blot with COX-2-specific antibody. (F) Recombinant human COX-2 was treated with SNP, and COX-2 activity was measured ($n = 3$, control: $V_{max} = 81.3 \pm 4.8$ nmol/min per mg, $K_m = 16.2 \pm 2.2$ μ M; SNP: $V_{max} = 132 \pm 6.5$ nmol/min per mg, $K_m = 17.0 \pm 2.0$ μ M). (G) Recombinant human COX-2 was treated with SNP, and its turnover rate (k_{cat}) was measured in the presence of various concentrations of sucrose. Data were expressed as k_{cat} -control over k_{cat} in each viscosity versus viscosity ratio.

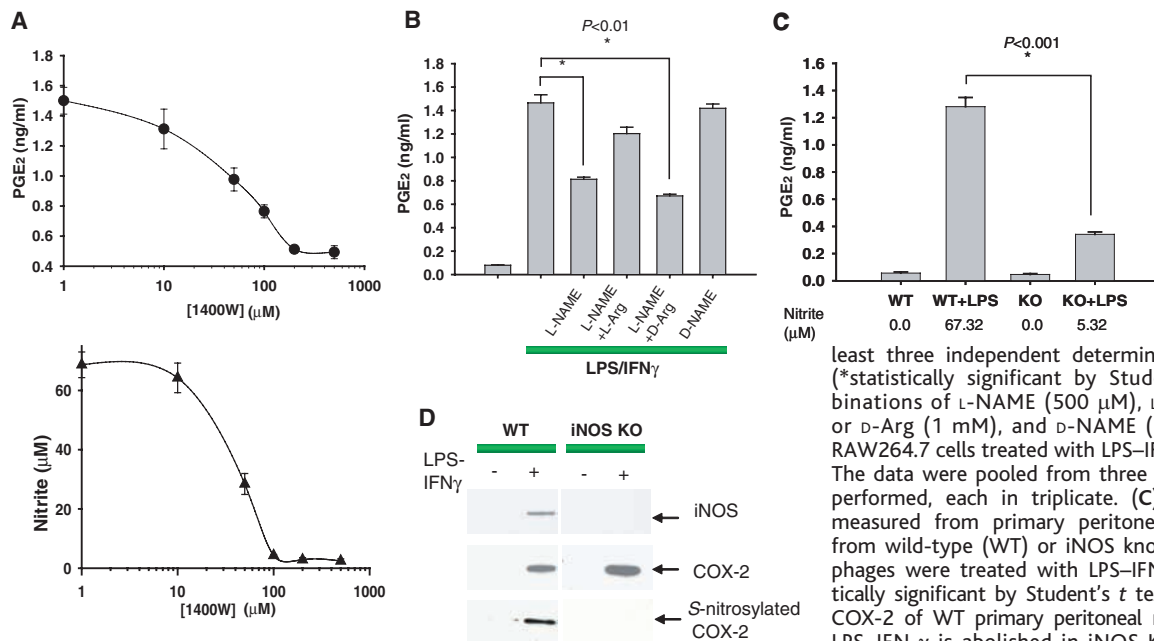


Fig. 3. Endogenously generated NO enhances COX-2 activity. (A) RAW264.7 cells were activated by LPS-IFN- γ and treated with various concentrations of iNOS inhibitor 1400W for 18 hours. The dose dependence of 1400W-mediated suppression of PGE₂ and nitrite was then measured. Data were pooled from at least three independent determinations, each in triplicate (*statistically significant by Student's t test). (B) Combinations of L-NAME (500 μ M), L-NAME + L-Arg (1 mM) or D-Arg (1 mM), and D-NAME (500 μ M) were added to RAW264.7 cells treated with LPS-IFN- γ . PGE₂ was measured. The data were pooled from three independent experiments performed, each in triplicate. (C) PGE₂ and nitrite were measured from primary peritoneal macrophages isolated from wild-type (WT) or iNOS knockout (KO) mice. Macrophages were treated with LPS-IFN- γ or untreated (*statistically significant by Student's t test). (D) S-Nitrosylation of COX-2 of WT primary peritoneal macrophages treated with LPS-IFN- γ is abolished in iNOS KO macrophages. All the

S-nitrosylated proteins were precipitated, and COX-2 was detected by Western blot with COX-2-specific antibody.

RAW 264.7 cells were transfected to express the N-terminal 483 amino acids or the C-terminal 120 amino acids of COX-2. LPS-IFN- γ treatment induced S-nitrosylation of the C-

terminal fragment (which contains three cysteines) but not the N-terminal fragment (fig. S6). To ascertain which of these three cysteines is responsible for augmented COX-2 activity, each

was mutated to serine. The mutation in which Ser is substituted for Cys⁵²⁶ (C526S) prevented activation of COX-2 by the NO donor SNP, whereas the C561S mutation did not (fig. S6).

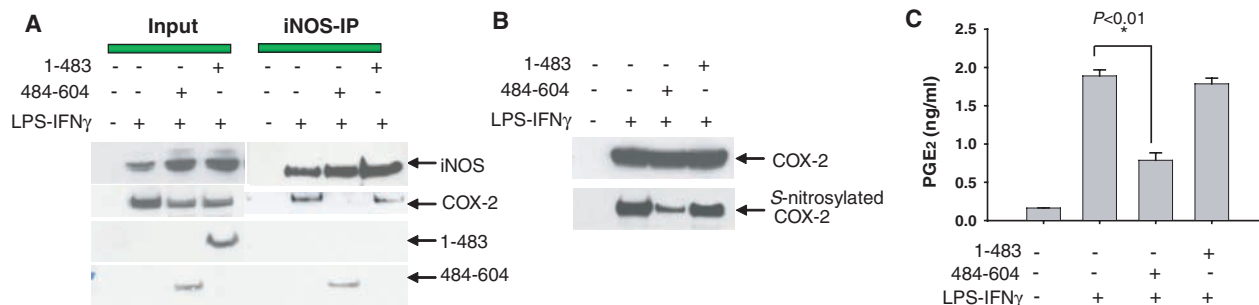


Fig. 4. COX-2-Myc fragment attenuates iNOS binding to COX-2 and NO-mediated activation of PGE₂ production. Transfected RAW264.7 cells expressing COX-2-Myc fragments 1 to 483 or 484 to 604 were treated with LPS-IFN- γ . (A) Cell lysates were immunoprecipitated with rabbit iNOS-specific antibody and analyzed by Western blot with antibodies against mouse iNOS, goat COX-2, and mouse Myc. (B) COX-2-Myc fragment (484 to 604) decreases S-nitrosylation of COX-2 in RAW264.7 cells. All the S-nitrosylated proteins were precipitated and COX-2 was detected by Western blot with COX-2-specific antibody. (C) Transfected RAW264.7 cells expressing the indicated COX-2 fragments were treated with LPS-IFN- γ . PGE₂ levels were measured and the data were pooled from three independent experiments performed, each in triplicate (*statistically significant by Student's *t* test). (D) PGE₂ and the indicated COX-2 fragments were visualized with confocal microscopy using antibodies against mouse Myc and rabbit PGE₂. Images of COX-2 (red) and PGE₂ (green) were superimposed to show colocalization. Nuclei were visualized with Hoechst staining (blue). In D1, arrows point to two RAW264.7 cells, only one of which is expressing the COX-2 fragment 484 to 604 (red). In D2, the same two cells are analyzed for presence of endogenous PGE₂ after activation of RAW264.7 cells by LPS-IFN- γ treatment. Immunofluorescent staining shows a reduction in the PGE₂ expression in cells expressing COX-2(484-604) compared with the nontransfected cell (D2). This observation contrasts with D4, where the arrows point to a nontransfected cell and a transfected cell expressing COX-2(1-483). D5 does not show a reduction of PGE₂ in the transfected cell as compared with the nontransfected cell.

The C555S mutation abolished enzyme activity, so the effects of NO stimulation could not be assessed. Individual mutation of the 13 cysteines in COX-2 did not detectably diminish total S-nitrosylation of the enzyme, which suggests that multiple cysteines can be S-nitrosylated, but only C526 is responsible for enzyme activation by NO.

To clarify the influence of NO on prostaglandin E₂ (PGE₂), a prostaglandin synthesized by COX-2 formation in a physiologic context, we examined RAW264.7 cells. The formation of PGE₂ in response to LPS-IFN- γ was inhibited by the iNOS inhibitor 1400W, with 50% reduction of PGE₂ formation at drug concentrations that provide 50% inhibition of iNOS activity (Fig. 3A). Specificity of the NO association was evident by inhibition of PGE₂ formation with the active L-isomer of the NOS inhibitor N-nitro-L-arginine methyl ester (L-NAME) but not by D-NAME; the effects of L-NAME were reversed by added L-arginine (Fig. 3B). Thus, about 50% of induced COX-2 activity is determined by S-nitrosylation.

As RAW264.7 cells are a continuous macrophage cell line that may not behave the same as macrophages in intact organisms, we used peritoneal macrophages from mice lacking iNOS. PGE₂ formation from macrophages of

mice treated with LPS-IFN- γ was reduced in the iNOS knockout mice by ~70%, in parallel with a similar reduction in nitrite formation by the macrophages (Fig. 3C) and a decrease in S-nitrosylated COX-2 (Fig. 3D). These observations concur with findings of decreased urinary PGE₂ in iNOS knockout mice (20).

We hypothesized that the increase in PGE₂ formation by iNOS activation reflects binding of iNOS to COX-2 to deliver NO in appropriate proximity for S-nitrosylation. To explore this possibility we blocked iNOS-COX-2 binding with the fragment of COX-2 (amino acids 484 to 604), which binds iNOS (Fig. 4A). Expression of COX-2(484-604) in transfected RAW264.7 cells abolished the coprecipitation of iNOS and COX-2. Instead, COX-2(484-604) associated with iNOS (Fig. 4A). Moreover, this interference of binding between COX-2 and iNOS by COX-2(484-604) decreased S-nitrosylation of COX-2 in RAW264.7 cells (Fig. 4B). The dominant-negative effect of COX-2(484-604) reduced PGE₂ formation by more than 50%, whereas expression of a COX-2 fragment of amino acids 1 to 483, which does not bind iNOS, failed to influence PGE₂ formation (Fig. 4, C and D).

In summary, our study establishes a physiologic binding interaction of iNOS and COX-2

bringing NO in proximity to COX-2, facilitating its S-nitrosylation and activation, and fitting with earlier findings that NOS inhibition decreases prostaglandin formation (9, 21). Our findings accord with recent evidence that many physiologic actions of NO require its delivery to molecular targets (12, 22, 23). Whereas scaffolding proteins such as CAPON (22) or PSD95 (23) link neuronal NOS, respectively, to Dexas1 (22) and N-methyl-D-aspartate receptors (23), iNOS and COX-2 bind directly. The molecular synergism between iNOS and COX-2 may represent a major mechanism of inflammatory responses. Drugs that block the iNOS-COX-2 interaction may be anti-inflammatory, synergizing with COX-2 inhibitors and permitting lower doses. As the binding site on iNOS is in the catalytic domain, derivatives of iNOS inhibitors that also prevent binding to COX-2 may decrease both NO and prostaglandin formation.

References and Notes

1. M. E. Turini, R. N. DuBois, *Annu. Rev. Med.* **53**, 35 (2002).
2. S. Moncada, *J. R. Soc. Med.* **92**, 164 (1999).
3. R. J. Flower, *Nat. Rev. Drug Discov.* **2**, 179 (2003).
4. E. J. Topol, *JAMA* **293**, 366 (2005).
5. T. P. Misko, J. L. Trotter, A. H. Cross, *J. Neuroimmunol.* **61**, 195 (1995).

6. I. Appleton, A. Tomlinson, D. A. Willoughby, *Adv. Pharmacol.* **35**, 27 (1996).
7. D. Salvemini et al., *J. Clin. Invest.* **93**, 1940 (1994).
8. J. R. Vane, Y. S. Bakhle, R. M. Botting, *Annu. Rev. Pharmacol. Toxicol.* **38**, 97 (1998).
9. D. Salvemini et al., *Proc. Natl. Acad. Sci. U.S.A.* **90**, 7240 (1993).
10. J. M. Braughler, C. K. Mittal, F. Murad, *J. Biol. Chem.* **254**, 12450 (1979).
11. S. R. Jaffrey, H. Erdjument-Bromage, C. D. Ferris, P. Tempst, S. H. Snyder, *Nat. Cell Biol.* **3**, 193 (2001).
12. D. T. Hess, A. Matsumoto, S. O. Kim, H. E. Marshall, J. S. Stamler, *Nat. Rev. Mol. Cell Biol.* **6**, 150 (2005).
13. R. M. Garavito, A. M. Mulchak, *Annu. Rev. Biophys. Biomol. Struct.* **32**, 183 (2003).
14. A. L. Tsai, C. Wei, R. J. Kulmacz, *Arch. Biochem. Biophys.* **313**, 367 (1994).
15. T. A. Kennedy, C. J. Smith, L. J. Marnett, *J. Biol. Chem.* **269**, 27357 (1994).
16. S. R. Jaffrey, S. H. Snyder, *Sci. STKE* **2001**, pl1 (2001).
17. F. Murad, C. K. Mittal, W. P. Arnold, S. Katsuki, H. Kimura, *Adv. Cyclic Nucleotide Res.* **9**, 145 (1978).
18. Y. Yang, J. Loscalzo, *Proc. Natl. Acad. Sci. U.S.A.* **102**, 117 (2005).
19. H. M. Lander, J. S. Ogiste, S. F. Pearce, R. Levi, A. Novogrodsky, *J. Biol. Chem.* **270**, 7017 (1995).
20. L. J. Marnett, T. L. Wright, B. C. Crews, S. R. Tannenbaum, J. D. Morrow, *J. Biol. Chem.* **275**, 13427 (2000).
21. D. Salvemini et al., *J. Clin. Invest.* **96**, 301 (1995).
22. M. Fang et al., *Neuron* **28**, 183 (2000).
23. H. C. Kornau, L. T. Schenker, M. B. Kennedy, P. H. Seeburg, *Science* **269**, 1737 (1995).
24. This work was supported by U.S. Public Health Service grant DA000266, Research Scientist Award DA00074 (to S.H.S.), and a Canadian Institute of Health Research fellowship (to S.F.K).

Supporting Online Material

www.sciencemag.org/cgi/content/full/310/5756/1966/DC1

Materials and Methods

Figs. S1 to S6

References

26 August 2005; accepted 11 November 2005

10.1126/science.1119407

Diversity and Function of Adaptive Immune Receptors in a Jawless Vertebrate

Matthew N. Alder,¹ Igor B. Rogozin,² Lakshminarayan M. Iyer,² Galina V. Glazko,³ Max D. Cooper,¹ Zeev Pancer^{4*}

Instead of the immunoglobulin-type antigen receptors of jawed vertebrates, jawless fish have variable lymphocyte receptors (VLRs), which consist of leucine-rich repeat (LRR) modules. Somatic diversification of the VLR gene is shown here to occur through a multistep assembly of LRR modules randomly selected from a large bank of flanking cassettes. The predicted concave surface of the VLR is lined with hypervariable positively selected residues, and computational analysis suggests a repertoire of about 10^{14} unique receptors. Lamprey immunized with anthrax spores responded with the production of soluble antigen-specific VLRs. These findings reveal that two strikingly different modes of antigen recognition through rearranged lymphocyte receptors have evolved in the jawless and jawed vertebrates.

An adaptive immune system based on lymphocytes bearing clonally diverse antigen-specific receptors first appeared at the dawn of vertebrate evolution ~500 million years ago. Within less than 40 million years in the Cambrian, both jawless and jawed vertebrates evolved mechanisms of lymphocyte receptor diversification that were radically different. Thus, jawed vertebrates rearrange immunoglobulin and T cell receptor (TCR) variable, diverse, and joining gene segments (VDJs) to generate highly diverse repertoires of T and B lymphocyte antigen receptors (1, 2). In contrast, lamprey and hagfish, jawless fish representatives of the oldest vertebrate taxon, assemble their VLRs from modular LRR units (3, 4). In the lamprey, a single incomplete germline VLR gene generates a diverse

repertoire of cell surface receptors through somatic rearrangement of LRR cassettes that flank the gene. Each lymphocyte thus assembles a VLR gene of unique sequence. Hagfish have two germline VLR genes, called VLR-A and VLR-B, that can generate equivalently diverse receptor repertoires (4). On the basis of the existence of a sizable repertoire of diverse lymphocyte receptors, we hypothesized that VLRs may serve as jawless fish equivalents of the anticipatory antigen receptors of jawed vertebrates.

The potential diversity of lamprey VLRs was estimated by analysis of 517 unique VLR sequences, including 129 previously reported sequences (3) and 388 new sequences derived mostly from animals immunized with the *Bacillus anthracis* spore coat (5). Analysis of the aligned VLR diversity regions revealed mixed clusters of sequences, with no exclusive clustering of VLRs from animals immunostimulated with particular antigens. The alignment was then converted into a matrix consisting of the individual types of constituent LRR modules (Fig. 1A). This included the 30 to 38 residue N-terminal LRR (LRRNT), 18-residue first LRR (LRR1), 24-residue LRRs (LRRVs), 13-residue connecting peptide (CP), and 48- to 65-residue C-terminal LRR (LRRCT). Noting that the terminal 24-residue LRR

module adjacent to the CP had a distinct sequence signature in 98% of the cases (fig. S1) (5), we designated this as the LRRV-end (LRRVe).

The data set was screened for repetitive occurrence of each type of LRR module, singly or as recurring pairs (Tables 1 and 2). Most pairs of adjoining LRRVs or LRRVe's were only observed once, but in some cases, repetitive pairs of LRRNT-LRR1 and CP-LRRCT were identified. These may represent VLRs that were assembled from multimodule genomic cassettes, such as one LRR1-LRRV-LRRV triplet previously identified in the VLR locus (3), or VLRs selected for certain structural conformations. However, 94% of the LRRNT-LRR1 and CP-LRRCT pairs are either unique or consist of the same pair of adjoining modules occurring three times or less in the VLR data set, and the pairing occurrence follows a random Poisson distribution (6). Most hagfish VLR-A modules were also found in random combinations ($n = 139$; tables S1 and S2), whereas the VLR-B sample ($n = 70$) was too small for reliable analysis. The potential diversity of the VLR repertoire was therefore calculated by considering individual LRR modules as independent recombination units. For the lamprey, we predict a potential repertoire of up to 10^{14} unique VLRs and up to 10^{17} for the hagfish VLR-A (5).

The number of LRR cassettes flanking the germline VLR gene is unknown. Thus far, 32 unique germline LRR modules have been identified in the partially sequenced lamprey VLR locus (3), and only 15 of these were identical to one of the 1568 modules from the VLR data set. To estimate the number of LRRV modules in flanking cassettes at the VLR locus, we used Monte Carlo simulations to predict at 95% confidence level an upper bound estimate of ~1500 lamprey LRRVs and ~2400 LRRVs for the hagfish VLR-A (5). These data suggest that the rearrangement process that yields mature VLR genes occurs by random selection of each module type from a large pool of genomic LRR modules.

The lamprey germline VLR gene of ~13 kb consists of three coding regions separated by two intervening sequences: (i) the signal peptide and 5' portion of LRRNT, (ii) the 5' portion of LRRCT, and (iii) the 3' portion of LRRCT

¹Howard Hughes Medical Institute, Departments of Medicine, Microbiology, Pediatrics, and Pathology, University of Alabama at Birmingham, Birmingham, AL 35294, USA. ²National Center for Biotechnology Information, National Library of Medicine, National Institutes of Health, Bethesda, MD 20894, USA. ³Stowers Institute for Medical Research, 1000 East 50th Street, Kansas City, MO 64110, USA. ⁴Center of Marine Biotechnology, University of Maryland Biotechnology Institute, Baltimore, MD 21202, USA.

*To whom correspondence should be addressed. E-mail: pancer@comb.umbi.umd.edu.